Journal of Instrumentation

In-situ remotely controllable ocean radiation monitoring system

To cite this article: S. Lee *et al* 2020 *JINST* **15** P06027

View the article online for updates and enhancements.


IOP ebooks™

Bringing together innovative digital publishing with leading authors from the global scientific community.

Start exploring the collection–download the first chapter of every title for free.

This content was downloaded from IP address 147.47.238.44 on 26/06/2020 at 02:37

Published by IOP Publishing for Sissa Medialab

Received: *February 13, 2020*
Revised: *April 29, 2020*
Accepted: *May 22, 2020*
Published: *June 25, 2020*

In-situ remotely controllable ocean radiation monitoring system

S. Lee,[a] J.S. Lee,[a,b] H.S. Kim,[c] J. Park,[c] S. Baek,[d] Y. Song,[d] J.-M. Seo[d] and S.M. Kim[d,1]

[a] *Department of Biomedical Sciences, Seoul National University,*
103 Daehak-Ro, Jongno-Gu, Seoul 03080, South Korea

[b] *Brightonix Imaging Inc., 25 Yeonmujang 5ga-Gil, Seongdong-Gu, Seoul 04782, South Korea*

[c] *Advanced Radiation Technology Institute, Korea Atomic Energy Research Institute,*
29 Geumgu-Gil, Jeongup 56212, South Korea

[d] *Maritime ICT R&D Center, Korea Institute of Ocean Science and Technology,*
385 Haeyang-Ro, Yeongdo-Gu, Busan 49111, South Korea

E-mail: smeekim@kiost.ac.kr

Abstract: Prompt in-situ monitoring of sea radiation contamination is crucial to prevent the sea from spreading radioactive materials to other parts of the world and the hazard of internal exposures in marine life and the human through food chain. In this paper, we evaluated the performance of a new ocean radiation monitoring robotic boat prototype system. The system featured real-time and on-site gamma spectroscopy with a portable detector of a CsI(Tl) crystal and a PIN diode carried by an unmanned surface vehicle. The system performed good energy linearity and energy resolution (21% at 662 keV). The efficiency and the minimum detectable activity (24 h acquisition) for underwater ^{137}Cs detection were 1.334×10^{-5} and 2.5 Bq/kg, respectively. We conducted a Monte Carlo simulation to estimate the detection performance with uniform and point source distributions. In the water tank experiments, we measured the count rates with differing depths of a ^{137}Cs point source. The maximum detectable distance was 50 cm according to both experiment and simulation results. Additionally, on-site experiment was conducted to test the operability of the system in a real sea. The overall study showed the feasibility of the system for in-situ ocean radiation monitoring.

Keywords: Radiation monitoring; Spectrometers

[1] Corresponding author.

© 2020 IOP Publishing Ltd and Sissa Medialab

https://doi.org/10.1088/1748-0221/15/06/P06027

2020 JINST 15 P06027

Contents

1 Introduction **1**

2 Methods and materials **2**
- 2.1 System specifications 2
- 2.2 Simulation 4
- 2.3 Detection performance test 5
- 2.4 Experiments 5

3 Results **7**
- 3.1 Detection performance test 7
- 3.2 Simulation 7
- 3.3 Experiments 9

4 Discussion **11**

5 Conclusion **11**

1 Introduction

It is reported that, as of 2019, there are 55 reactors under construction and 450 in operation worldwide [1]. Furthermore, some countries have recently started building floating nuclear power plants that can be transferred to areas across the sea to provide electricity [2]–[4]. In the entire process, from operation of the new reactors to their handling under shutdown stage, nuclear safety needs to be periodically evaluated by monitoring the radiation level near the power plants. We need to be aware of the potential hazard of radiation leaking into the sea water associated with the disposal of nuclear wastes or the failure of the reactor coolant system, as happened during the Fukushima Dai-ichi Nuclear Power Plant (FDNPP) accident [5]. Unlike radiation contamination on land, marine radiation contamination can spread all over the world by ocean currents and long-lived isotopes is possible to affect marine life or human through food chain [6]–[10]. Thus, the nation operating nuclear power plants need to monitor periodically the marine radiation activity changes.

A typical method to monitor ocean radiation is by measuring the radioactivity of the sampled sea water in the laboratory. The Center for Marine and Environmental Radiation has conducted a project measuring the radiation levels across the Pacific Ocean from Japan to the Pacific Coast of North America [11]. Similarly, an integrated environmental radiation monitoring network service from the Korea Institute of Nuclear Safety (KINS) updates the ocean radiation level information every three months at 27 ocean spots around South Korea [12]. KINS increased the annual survey frequency and water-sampling spot number after FDNPP accident, however it is still insufficient to monitor the vast territorial waters of South Korea. The typical method is ineffective to extensive

2020 JINST 15 P06027

prompt survey because of time- and cost-consuming processes of carrying and analyzing large amount of sea water. Additional in-situ monitoring has been emphasized for prompt monitoring of the change of the marine radiation activity levels and for quick and right preparedness from the accidental events in near-land or neighbor countries.

In-situ gamma-ray measurement has been emphasized for prompt monitoring and preparedness of emergency. Most in-situ radiation detectors for inspecting marine environment are scintillator-based detectors. Considering low cost and high efficiency, NaI(Tl) of $3'' \times 3''$ composed with photomultiplier tube (PMT) is common [13]–[19]. HPGe was also used with NaI(Tl) detector for additional high energy resolution [20]. However, HPGe needs a coolant system, which should be unstable in a variety of ocean environment. Furthermore, NaI(Tl) scintillator is hydroscopic and PMT would be unstable in marine environment and needs high voltage. Recently, other scintillators such as $LaBr_3$:Ce and $CeBr_3$ are investigated for marine radiation spectra measurements [21, 22]. $LaBr_3$:Ce and $CeBr_3$ are effective for high efficiency and high energy resolution, while these have intrinsic radiation background disturbing the interested oceanic radiation spectra. These scintillator-based detectors are deployed in several platforms. Some are equipped to stationary observation stations or buoys for long-term radioactivity monitoring [23]–[25]. Other well-known in-situ equipment include an eel-like system in which the detector is towed with a long cable from a ship for sea floor measurements [20, 26–28], but both methods have limited mobility for seawater radioactivity survey. For flexible mobility in a variety of marine environments, some radiation detecting robotic systems were reported to survey radioactivity in waters [29]–[31].

An in-situ, remotely controllable monitoring system is required for frequent, accurate, safe, and cost-effective monitoring of the ocean radiation level. In this paper, we have developed a prototype system of an unmanned surface vehicle (USV) equipped with a radiation detector and communication devices to measure real-time ocean radiation levels in the desired regions from the coast to the far sea. A portable gamma-ray detector which has a simple structure and requires a low supply voltage was used to maximize the mobility of the system. The in-situ monitoring system can be applicable to early warning system for daily continuous marine inspection or to port radiation survey of the discharged ballast water of vessels from foreign countries having high risks of radiation contamination. We conducted simulations and experiments to evaluate the detectability of the prototype system for 662 keV gamma-rays emitted from ^{137}Cs, which is a major fission product of uranium.

2 Methods and materials

2.1 System specifications

The conceptual design of the ocean radiation monitoring system is described in figure 1. We used a detector which was designed and fabricated by Korea Atomic Energy Research Institute for application in various radiation detection fields [32, 33]. The detector consisted of a single $10 \times 10 \times 20\,\text{mm}^3$ CsI(Tl) scintillation crystal coupled with a silicon PIN diode and built-in electronic circuits with an amplifier and shaper (figure 2(a)). A voltage of 9 V was applied to the detector from a shipped battery. Compared to the conventional state-of-art photosensors such as photomultiplier tube and silicon photomultiplier, the PIN diode we used was suitable for the system because it required low supply voltage and it was robust to temperature variance and external impact.

2020 JINST 15 P06027

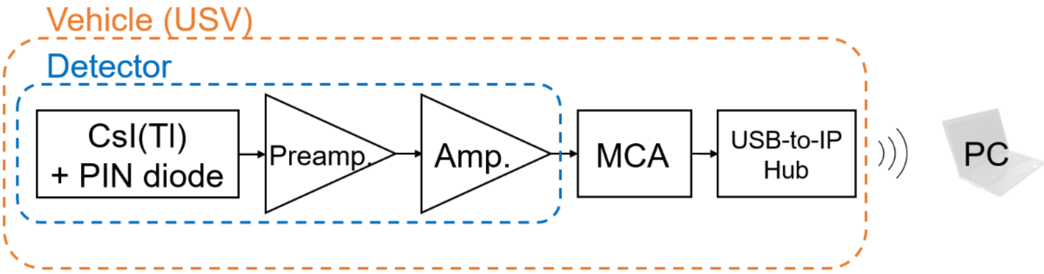

Figure 1. Conceptual diagram of the ocean radiation monitoring system.

Figure 2. Pictures of system configuration. (a) Radiation detector with built-in electronics, (b) detector and MCA shielded with an aluminum case, (c) placement of aluminum case inside USV, and (d) whole USV.

A multichannel analyzer (MCA; ORTEC, U.S.A.) was connected to the detector by a LEMO cable and generated an energy spectrum of the detected analog radiation signals with a resolution of 12-bits. The spectrum data from the MCA were transferred through a USB-over-IP hub to a remote laboratory PC via a wireless network. The detector and the MCA were shielded by an aluminum case with a thickness of 2 mm to prevent interferences caused by analog noise from other electronic equipment (figure 2(b)). As shown in figure 2(c), the aluminum case was shipped in a USV which was remotely controllable.

The size of the USV body was approximately $170 \times 38 \times 28\ \mathrm{cm}^3$, and the material of the body was carbon fiber reinforced polymer (FRP) as shown in figure 2(d). The lifetime of the fully charged

2020 JINST 15 P06027

battery was 4 h under operation, and the maximum communication distance was 8 km. The USV was equipped with two motors at the rear. The maximum moving speed of the USV was 16 km/h. Movement of the USV was manually operated by a customized remote controller or automatically operated along the predefined path.

2.2 Simulation

We used a Geant4-based Monte Carlo simulation toolkit [34] to estimate the detection performance of the radiation monitoring system (figure 3(a)). Table 1 summarizes the properties of the USV, the shielding case, and the crystal that were simulated in this study. The shape of the USV was simplified to that of a box. The aluminum case was attached to the center of the inner bottom of the USV, and the crystal was placed 3 cm above the center of the inner bottom of the aluminum case. The USV was placed on the surface of a $1500 \times 1000 \times 600\,\mathrm{cm}^3$ water tank with the bottom half sunk.

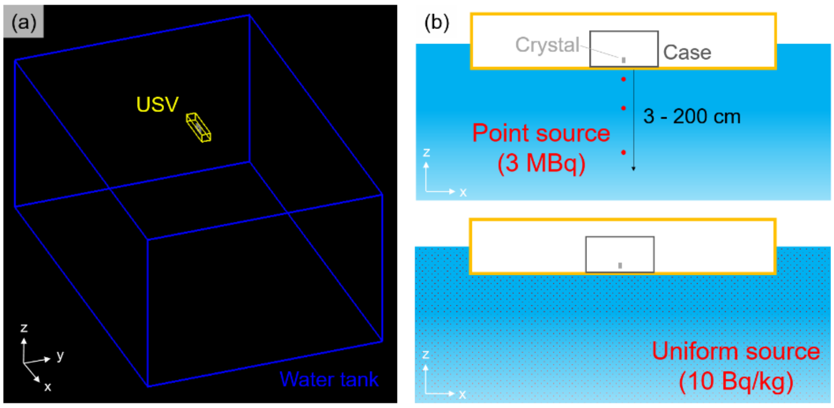

Figure 3. Simulation setup. (a) USV floated in a water tank, (b) local and uniform source distributions (figures in (b) not drawn to scale).

Table 1. Geometric details of system components for Monte Carlo simulation.

	Material	Density (g/cm^3)	Size	Form	Shell thickness
USV body	Carbon	1.9	$170 \times 38 \times 28\,\mathrm{cm}^3$	Hollow shell	1 cm
Case	Aluminum	2.7	$380 \times 184 \times 50\,\mathrm{mm}^3$	Hollow shell	2 mm
Crystal	CsI	4.51	$10 \times 10 \times 20\,\mathrm{mm}^3$	Solid	—

Two different source distributions were tested in the simulation (figure 3(b)). First, the ^{137}Cs source was uniformly distributed in the water tank with a radioactivity concentration of 10 Bq/kg, which is still far greater than an actual ocean radiation level. The data were acquired for 1 h. Second, the ^{137}Cs point source was placed at various distances, between 3 and 200 cm, from the bottom center of the USV. The radioactivity was 3 MBq, and the acquisition time at each position of the

2020 JINST 15 P06027

source was 5 min. For both the simulation setups, we counted the number of detected 662 keV gamma-rays applying an energy window of [520, 800] keV, which corresponded to two times the energy resolution in FWHM around 662 keV which was measured in section 2.3.

2.3 Detection performance test

Energy calibration of the radiation detector was conducted outside the USV. The MCA was directly connected to the lab PC, and a single point source was attached to the front side of the detector. We obtained the energy spectra of ^{22}Na, ^{137}Cs, and ^{60}Co which generate peaks at 511 keV, 662 keV, and 1332.5 keV, respectively, for 15 minutes, and evaluated the energy linearity. We did not use the 1173 keV peak of the ^{60}Co source as it was hardly distinguishable in the spectrum due to low radioactivity of the source. We measured the energy resolution of the detector at each peak energy in full width in half maximum (FWHM).

Detection efficiency was evaluated as a proportion of the number of the detected gammas to the number of disintegrations of uniformly distributed ^{137}Cs within an effective volume. Here, the term "effective volume" denotes a volumetric range where a uniformly distributed sources are detectable [35, 36]. In this study, we set the effective volume as a hemisphere with a radius of 50 cm from the crystal floated on the water as shown in figure 4(b) because the simulation results in section 3.2 show that source farther than 50 cm from the detector are hardly detectable. ^{137}Cs solution uniformly distributed in a volume larger than 50 cm-radius sphere was not available, thus we indirectly measured the efficiency of ^{137}Cs with a feasible test setup and simulation. We first acquired 511 keV data from ^{18}F-FDG distributed within a cylindrical container which has a radius of 11 cm and a height of 18 cm. To mimic the realistic test setup, we stacked the detector in the aluminum case and a carbon FRP board of $30 \times 30 \times 1\ \mathrm{cm}^3$ on the container as shown in figure 4(a). The initial activity concentration of ^{18}F was 11.15 MBq/kg, and the total acquisition time was 48 hours. We selected time points between 16 to 20 hours for counting ^{18}F disintegrations and the detected 511 keV gammas when pulse pile-up effect and background count rate were insignificant. The identical test setup of ^{18}F was simulated (figure 4(b)) and then the experiment-to-simulation efficiency factor was calculated by the ratio of the experimental efficiency to the simulation efficiency. Assuming a linear conversion relationship between the simulation and the experiment, the efficiency factor was multiplied to the ^{137}Cs detection efficiency measured from the simulation in section 2.2 using the effective volume of 50 cm hemisphere (figure 4(b)).

We assessed minimum detectable activity (MDA) of our system for underwater ^{137}Cs measurement. A background measurement was conducted for 24 hours recording the energy spectrum every 5 min. The MDA was calculated by Currie formula [37] with a confidence level of 95%:

$$\mathrm{MDA} = \frac{2.71 + 4.65\sqrt{N_B}}{\varepsilon V P_\gamma t}\ (\mathrm{Bq/kg}),$$

where N_B, ε, V, P_γ, and t denote background counts, efficiency, effective volume, probability of 662 keV gamma-ray emission (94.6%), and acquisition time, respectively.

2.4 Experiments

We performed an experiment inside a water tank facility in the Underwater Test and Evaluation Center of the Korea Institute of Ocean Science and Technology (KIOST) in Pohang, Korea, and

2020 JINST 15 P06027

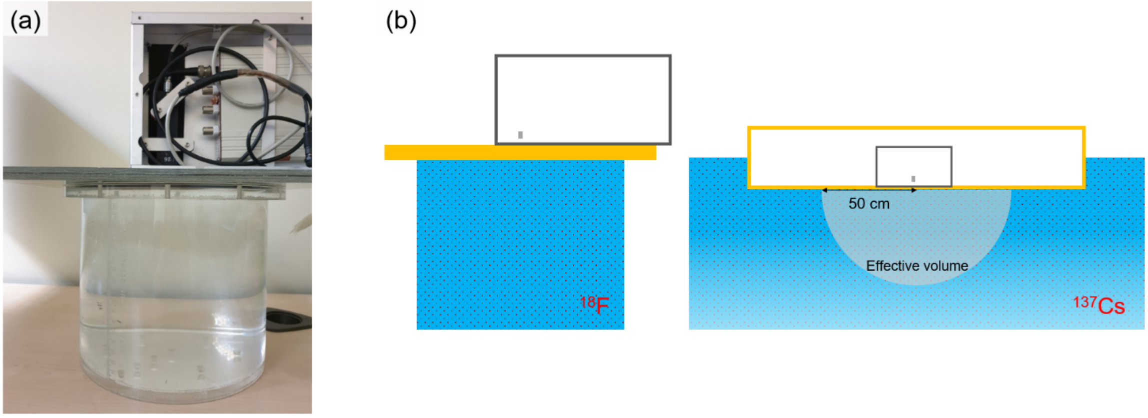

Figure 4. (a) Experiment and (b) simulations for system efficiency measurement. (a) ^{18}F solution was uniformly distributed inside a container. (b-left) The same configuration to (a) was simulated. (b-right) In a uniform ^{137}Cs solution, a 50 cm hemisphere was set as effective volume to count ^{137}Cs disintegrations. (Figures in (b) not drawn to scale).

the size of the tank was $35 \times 20 \times 8\,\text{m}^3$. First, we obtained the background spectrum data without any radioactive source. A ^{137}Cs point source was tied with a rope at the different distances of 3, 10, 25, 50, 100, and 200 cm from the bottom surface of the USV (figure 5(a)). We tested two different source activities of 3 MBq and 1 MBq. The USV was floated on the center of the water tank without movement (figure 5(b)). The time duration for the data acquisition was 5 min for each source radioactivity and distance setup. We measured the count rates within an energy window of [520, 800] keV around the pre-calibrated 662 keV peak.

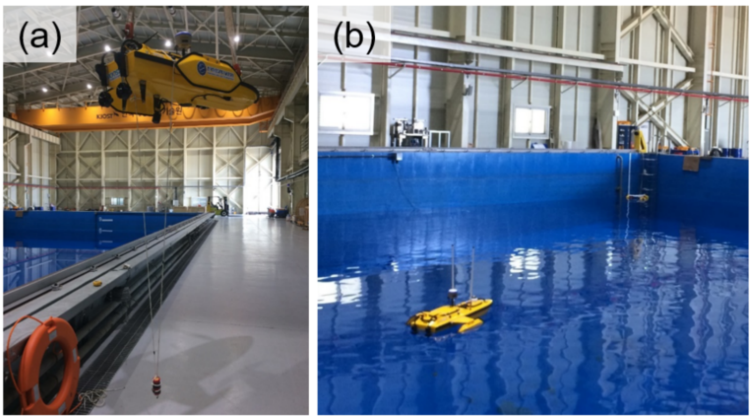

Figure 5. Pictures of the water tank experiment. (a) ^{137}Cs point source was tied to the USV with a rope. (b) USV floating in the water during data acquisition.

Additionally, to demonstrate the operability of the system in the real sea, we tested the radiation monitoring system in front of the Marine Living Resources Station of KIOST in Tongyoung, which is located on eastern sea in Korea (figure 6(a)). We obtained the data during the 20 min in which the USV moved automatically along the path shown in figure 6(b) up to 200 m away from the station [38]. USV can be operated under either an autopilot mode or a manual mode and has dual

2020 JINST 15 P06027

thrusters that propel itself. For auto pilot, we used “MissonPlanner” software that enable us to set a route of USV as we want. The detailed description how to set a route of USV with “MissonPlanner” is described in ref. [39]. If the route setting is finished, this information is transmitted to USV via radio frequency communication. It is identified whether it is successfully transmitted though “MissionPlanner”. USV successfully receiving the information can be operated under the autopilot mode. In our experiments, the distance between path lines and the speed of USV are set as 5 m and 4 km/h, respectively.

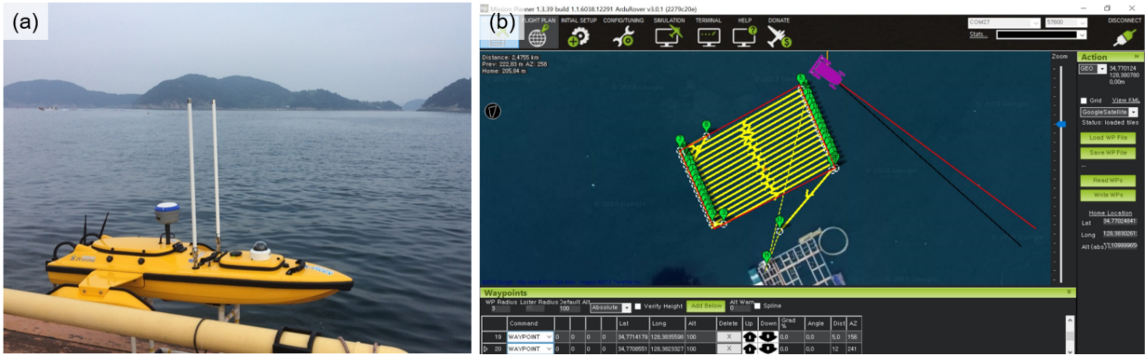

Figure 6. On-site experiment. (a) Picture of USV at the shore. (b) Screenshot of the GPS software controlling the USV route during the data acquisition.

3 Results

3.1 Detection performance test

Energy spectra of the background and the three point sources (^{22}Na, ^{137}Cs, and ^{60}Co) obtained by the detector are shown in figure 7(a). The 662 keV peak, which we have used in this paper, was appeared around the channel number 191 in the MCA spectrum. In the background spectrum, the counts were high in the low energy channels because of intrinsic noise contributed by the detector and the MCA, but the noise was insignificant around 662 keV. The background count rate within the energy window of [520, 800] keV was 0.29 cps, and it was subtracted from the source count rates measured in the experiments conducted in the water tank. As in figure 7(b), the peak channel numbers of the three sources were linearly correlated to the gamma-ray energies, and the energy resolution of the system was 21% in FWHM for ^{137}Cs (figure 7(c)).

F-18 detection efficiencies assessed from the experiment and the simulation were 1.398×10^{-4} and 1.441×10^{-4}, respectively and the experiment-to-simulation efficiency factor was 0.97. The converted experimental efficiency for ^{137}Cs was 1.334×10^{-5} from the simulation efficiency of 1.375×10^{-5}.

The MDA for ^{137}Cs detection was 51.3 and 2.5 Bq/kg for 5 min and 24-hour acquisitions. As shown in figure 8, increasing the acquisition time achieved lower MDA due to decreasing the statistical system noise.

3.2 Simulation

In the uniform source distribution setup with a radioactivity concentration of 10 Bq/kg, the measured count rate was 0.036 cps. Most of the detected events, which fell into the energy window, originated

2020 JINST 15 P06027

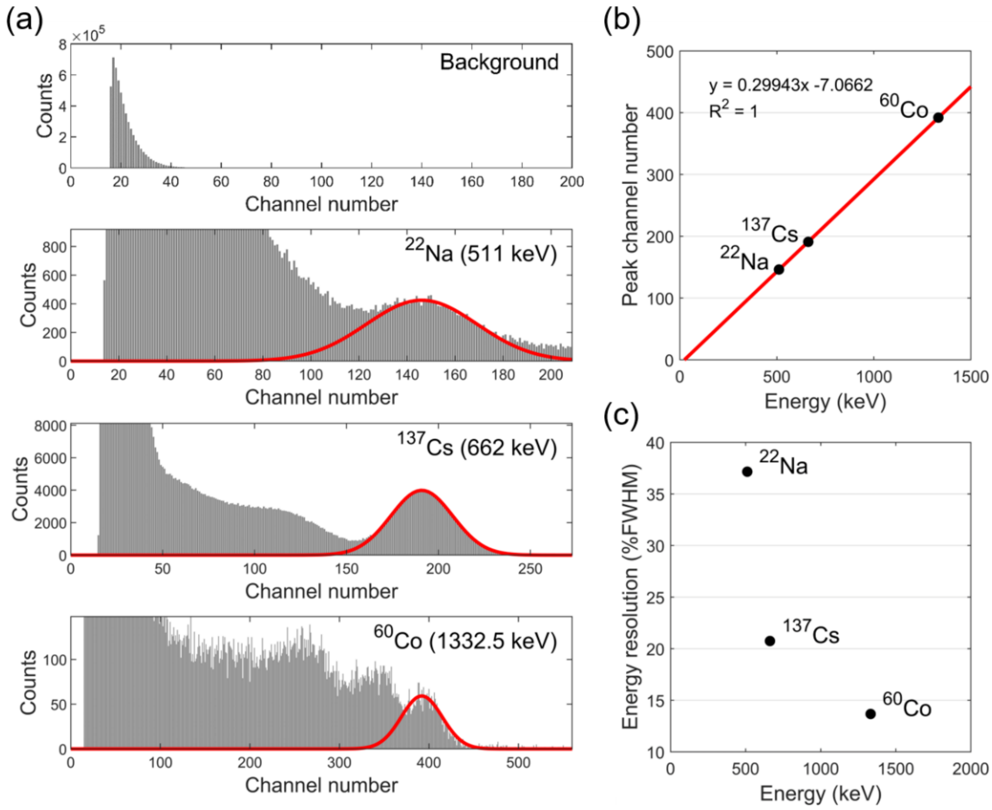

Figure 7. Energy calibration test of the detector. (a) Energy spectra of background, ^{22}Na, ^{137}Cs, and ^{60}Co radioactive point sources, (b) energy-to-channel calibration, and (c) energy resolutions of three sources.

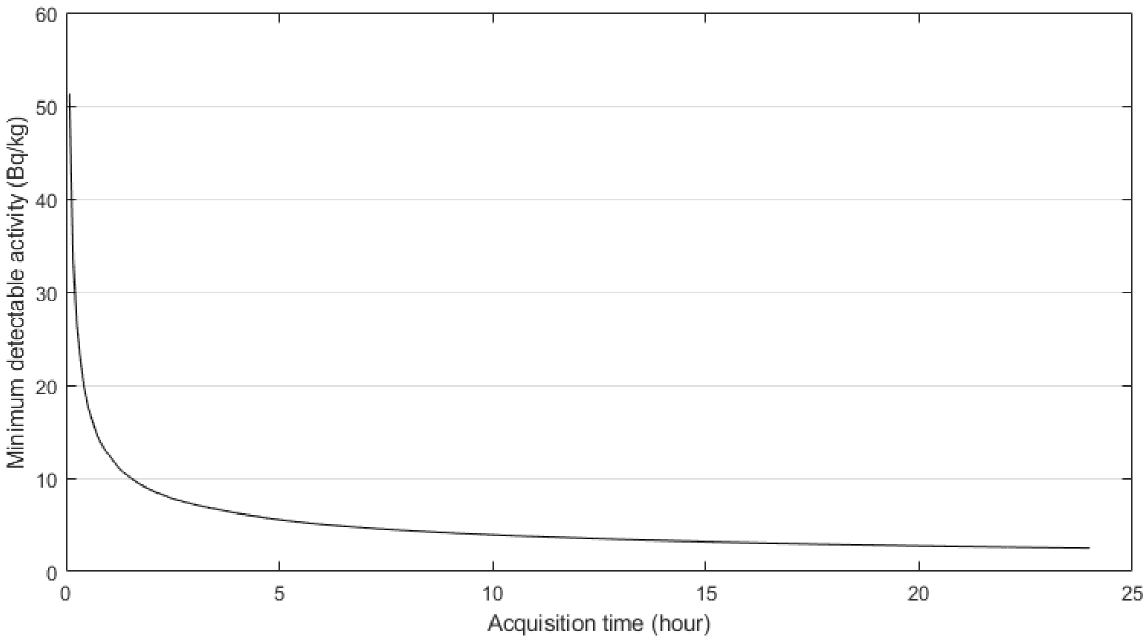

Figure 8. Measured MDA as a function of blank acquisition time.

2020 JINST 15 P06027

from ^{137}Cs sources within 50 cm far from the detector (figure 9(a)). Without the application of the energy window, the system was able to detect the only those sources that were within a distance of 100 cm. Limitations in the detection efficiency and detectable distance were due to the high probability of absorption and Compton scattering in the water, the aluminum case, and the body of the USV. As shown in figure 9(b), 96% of the detected gamma-rays underwent one or more Compton scatterings before reaching the detector mounted inside the USV.

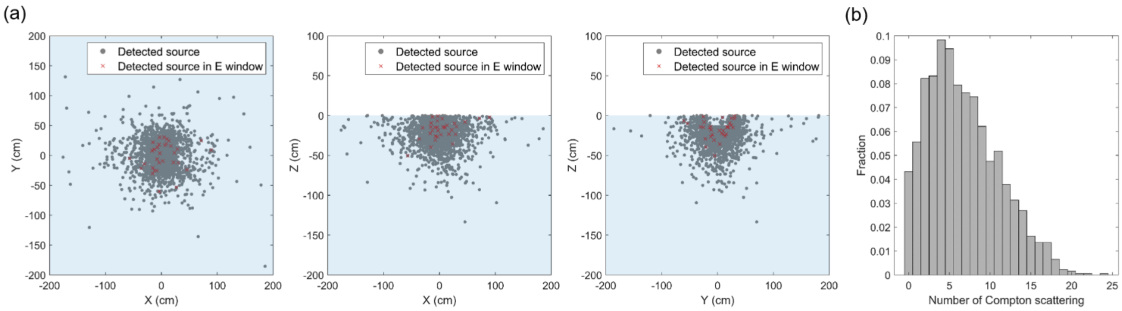

Figure 9. Simulation results of uniform ^{137}Cs distribution of 10 Bq/kg. (a) X–Y, X–Z, and Y–Z planes showing the emission sites of the detected source (blue-colored area indicates the water). (b) Histogram of number of Compton scatterings of gamma rays before reaching the detector.

As the point source was placed farther from the detector, the detected counts largely decreased because the gamma-rays were highly attenuated by the water (figure 10). Additionally, the cross-sectional area of the crystal facing the source was inversely proportional to the square of the distance between the source and the detector. Counts for the valid events under the energy window of [520, 800] keV were significant for distances up to 50 cm. No events were detected when the distance was larger than 100 cm, even when no energy window was applied.

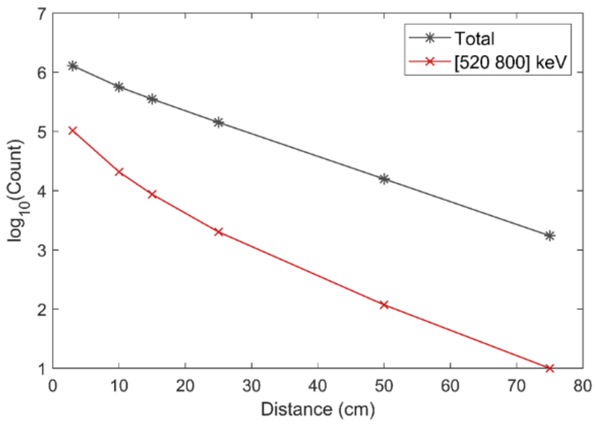

Figure 10. Count of the detected events in log scale at different ^{137}Cs source-to-USV distances in the simulation with and without applying the energy window of [520, 800] keV.

3.3 Experiments

Energy spectra obtained in the experiments conducted in the water tank are summarized in figure 11. As the distance of the source from the USV increased, the detected counts decreased and the 662 keV

2020 JINST 15 P06027

peak was hard to distinguish from the counts at other energies. The peak was distinguishable when the distance was less than 50 cm, while the spectra were similar to the background spectrum when the source was placed farther than 100 cm. The count rates of 3 MBq and 1 MBq sources of dotted and solid black lines were consistently proportional in distances less than 50 cm (figure 12). Therefore, the linearity between the detected counts and the source radioactivity was preserved when a significant number of events was detected under the peak region in the energy spectrum.

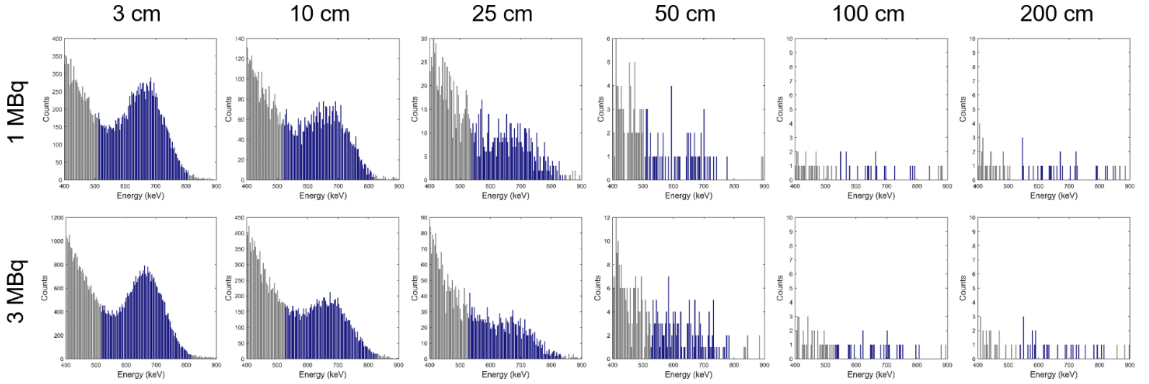

Figure 11. ^{137}Cs energy spectra of different distance (3 to 200 cm) and radioactivity (1 and 3 MBq) configurations in water tank experiment. Blue-colored region indicates the events fell into the energy window of [520, 800] keV.

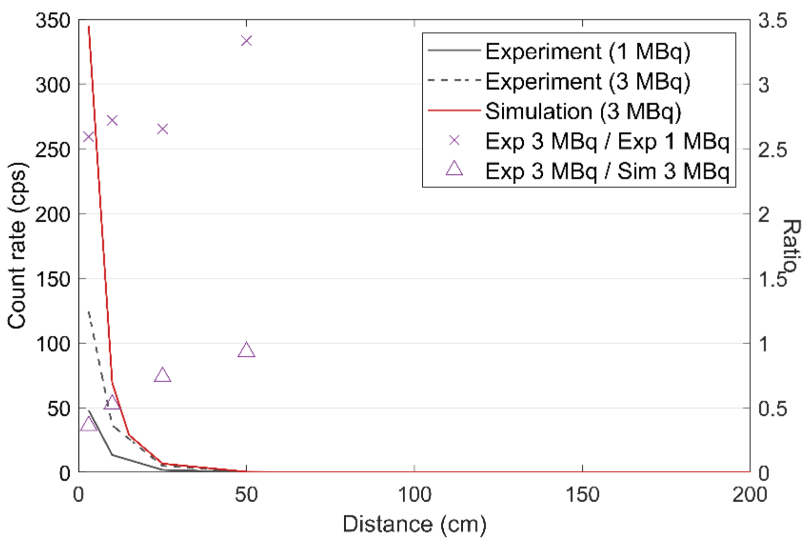

Figure 12. Count rates and count rate ratios of ^{137}Cs point source measured from the experiment and simulation in each distance and activity configuration.

The simulation and the experimental results were compared in figure 12. In both simulation and experiment, no event was detected when the distance was longer than 50 cm, which indicated that the maximum detectable distance of the system was roughly 50 cm. However, the count rates measured in the simulation were found to be significantly higher than the experimental count rates for the short distance configurations of 3 cm and 10 cm due to several limitations. Attenuation of

2020 JINST 15 P06027

the gamma-ray was dominant in the USV when the source was located nearby, but the realistic shape of the body and the arrangement of the other components, such as the battery and sensing devices equipped to the USV, were not considered in the simulation. Also, the misalignment of the point source and the detector largely contributed to the difference between the experiment and simulation results in short source-to-USV distances. However, the ratio of the count rates between the experiment and simulation tended to unity as the distance increased and attenuation became dominant in the water.

In the on-site experiment, events were hardly detected around 662 keV during the 20 min acquisition. The count rate without background subtraction was 0.05 cps which was comparable to the background system noise level.

4 Discussion

We herein demonstrated the successful operation of our prototype in-situ ocean radiation monitoring system. With a simple configuration of the radiation detector, we could instantaneously measure the energy spectra of underwater ^{137}Cs sources. Due to its compact design and portability, the radiation detector can be used in any type of unmanned vehicle, besides a USV, for a wide range of purposes. Also, the automatic movement of the USV was advantageous in approaching the desired region and avoiding unexpected obstacles. Additionally, dynamic measurement while moving the USV can enable easy localization of a highly radioactive source.

The most challenging issue was the considerable attenuation of the photons inside the water, which limited the detection efficiency of the system. Both the simulation and experimental results showed that sources farther than 50 cm from the detector were barely detected. The results show that good mobility of the system to easily access the desired region is a powerful benefit of this system. In this study, the movement of the USV was restricted to shallow water, but the next-generation system is planned to feature deep-sea operation and underwater communication.

MDA and signal-to-noise ratio of our detector need to improve to overcome the attenuation problem. According to MDA measurements, the system is capable of spontaneously detecting severe accidents such as the FDNPP accident which resulted in an estimated ^{137}Cs concentration of up to 68 kBq/kg in the sea water [40], or probable dissemination of contamination with activity concentration higher than the MDA of the system. However, as the annual average of the ^{137}Cs concentration is 1.64 to 1.88 mBq/kg [41], the present system is not sensitive to variation in the daily radiation level. In order to monitor the early stage of change in ocean radioactivity and daily radioactivity fluctuation, MDA should be increased by more than 1500 times. Based on this study, the detector would be composed of crystals with a large cross-section and high stopping power, and a photosensor with a large gain and low noise level. Using a crystal which performs a superior energy resolution would enable the system to cover different radionuclides in gamma spectroscopy.

5 Conclusion

Through simulations, experiments, and on-site test, we evaluated the initial performance of our newly developed in-situ ocean radiation monitoring prototype system and showed the potential feasibility to measure ocean radiation level. We tested the detection performances and experimented varying

2020 JINST 15 P06027

the position of a ^{137}Cs point source from the system. From Monte Carlo simulation, we estimated the detection efficiency of the system and observed a high frequency of attenuation of the 662 keV gamma-rays. Both the simulation and experimental results demonstrated that the system is able to detect 662 keV from underwater ^{137}Cs sources within 50 cm from the USV. According to our measurements of ^{137}Cs detection efficiency and MDA, the low detectability remained as a major limitation of the system. Our initial results will be a benchmark to enhance the performance of next-generation system. To improve system performance, it is necessary to choose a detector having a larger cross-section, higher gain, and better energy resolution.

Acknowledgments

This work was supported by research grants from Korea Institute of Ocean Science and Technology (PE99832), Basic Science Research Program through the National Research Foundation of Korea (NRF) funded by the Ministry of Education (NRF-2018R1D1A1B07049296), and nuclear R&D program of the Ministry of Science and ICT of Korea (NRF No. 2019M2A2A4A05031483). Our work also received technical support from the Radiation Equipment Fabrication Center in the Korea Atomic Energy Research Institute.

References

[1] https://pris.iaea.org/pris/.

[2] J. Buongiorno, J. Jurewicz, M. Golay and N. Todreas, *The offshore floating nuclear plant concept*, *Nucl. Technol.* **194** (2016) 1.

[3] http://www.rosenergoatom.ru/en/about-us/innovative-activities/floating-npp/.

[4] https://www.asiatimes.com/2019/03/article/ocean-going-nuclear-plants-for-south-china-sea/.

[5] IAEA, *The Fukushima Daiichi Accident*, IAEA, Vienna Austria (2015).

[6] Q. Schiermeier, *Radiation release will hit marine life*, *Nature* **472** (2011) 145.

[7] K.O. Buesseler et al., *Fukushima-derived radionuclides in the ocean and biota off Japan*, *PNAS* **109** (2012) 5984.

[8] T. Wada et al., *Effects of the nuclear disaster on marine products in Fukushima*, *J. Environ. Radioact.* **124** (2013) 246.

[9] J.N. Smith, R.M. Brown, W.J. Williams, M. Robert, R. Nelson and S.B. Moran, *Arrival of the Fukushima radioactivity plume in North American continental waters*, *Proc. Nat. Acad. Sci.* **112** (2014) 1310.

[10] H. Okamura, S. Ikeda, T. Morita and S. Eguchi, *Risk assessment of radioisotope contamination for aquatic living resources in and around Japan*, *Proc. Nat. Acad. Sci.* **113** (2016) 3838.

[11] http://ourradioactiveocean.org.

[12] http://iernet.kins.re.kr/.

[13] C. Tsabaris and I. Thanos, *An underwater sensing system for monitoring radioactivity in the marine environment*, *Mediterr. Mar. Sci.* **5** (2004) 125.

2020 JINST 15 P06027

[14] I. Osvath, P.P. Povinec, H.D. Livingston, T.P. Ryan, S. Mulsow and J.-F. Commanducci, *Monitoring of radioactivity in NW Irish Sea water using a stationary underwater gamma-ray spectrometer with satellite data transmission*, *J. Radioanal. Nucl. Chem.* **263** (2005) 437.

[15] L. Sartini et al., *GEMS: Underwater spectrometer for long-term radioactivity measurements*, *Nucl. Instrum. Meth. A* **626–627** (2011) S145.

[16] Y. Zhang, B. Wu, D. Liu, Y. Zhang and Y. Cheng, *Development and deployment of an autonomous sensor for the in-situ radioactivity measurement in the marine environment*, *Appl. Radiat. Isot.* **142** (2018) 181.

[17] A. Naumenko et al., *Autonomous NaI(Tl) gamma-ray spectrometer for in situ underwater measurements*, *Nucl. Instrum. Meth. A* **908** (2018) 97.

[18] J. Wang, Y. Zhang, D. Liu, B. Wu, Y. Zhang and H. Jiang, *Automated spectra analysis of in situ radioactivity measurements in the marine environment using NaI(Tl) detector*, *Appl. Radiat. Isot.* **141** (2018) 88.

[19] M. Fejgl and M. Hýža, *Development of an autonomous station for measurements of artificial gamma activity in surface water bodies*, *J. Environ. Radioact.* **204** (2019) 42.

[20] P.P. Povinec, I. Osvath and M.S. Baxter, *Underwater gamma-spectrometry with HPGe and NaI(Tl) detectors*, *Appl. Radiat. Isot.* **47** (1996) 1127.

[21] Z. Zeng et al., *Optimization of an underwater in-situ $LaBr_3$:Ce spectrometer with energy self-calibration and efficiency calibration*, *Appl. Radiat. Isot.* **121** (2017) 101 [`arXiv:1608.01109`].

[22] C. Tsabaris et al., *Development and optimization of an underwater in-situ cerium bromide spectrometer for radioactivity measurements in the aquatic environment*, *J. Environ. Radioact.* **204** (2019) 12.

[23] C. Wedekind, G. Schilling, M. Grüttmüller and K. Becker, *Gamma-radiation monitoring network at sea*, *Appl. Radiat. Isot.* **50** (1999) 733.

[24] I. Osvath, P.P. Povinec, L. Huynh-Ngoc and J.-F. Comanducci, *Underwater gamma surveys of Mururoa and Fangataufa lagoons*, *Sci. Total Environ.* **237–238** (1999) 277.

[25] U.R. Aakenes, *Radioactivity monitored from moored oceanographic buoys*, *Chem. Ecol.* **10** (1995) 61.

[26] I. Osvath and P.P. Povinec, *Seabed γ-ray spectrometry: applications at IAEA-MEL*, *J. Environ. Radioact.* **53** (2001) 335.

[27] D.G. Jones, *Development and application of marine gamma-ray measurements: a review*, *J. Environ. Radioact.* **53** (2001) 313.

[28] B. Thornton, S. Ohnishi, T. Ura, N. Odano and T. Fujita, *Continuous measurement of radionuclide distribution off Fukushima using a towed sea-bed gamma ray spectrometer*, *Deep Sea Res. Part I* **79** (2013) 10.

[29] M. Hattori, M. Okano and O. Togawa, *Sea bottom gamma ray measurement by NaI(Tl) scintillation spectrometers installed on manned submersibles, ROV and sea bottom long term observatory*, in proceedings of the *2000 International Symposium on Underwater Technology (Cat. No.00EX418)*, Tokyo, Japan, 23–26 May 2000, pp. 212–217.

[30] G.A. Wilde, R.R. Murphy, D.A. Shell and C.M. Marianno, *A man-packable unmanned surface vehicle for radiation localization and forensics*, in proceedings of the *2015 IEEE International Symposium on Safety, Security, and Rescue Robotics (SSRR)*, West Lafayette, IN, U.S.A., 18–20 October 2015, pp. 1–6.

2020 JINST 15 P06027

[31] K. Groves, A. West, K. Gornicki, S. Watson, J. Carrasco and B. Lennox, *MallARD: An autonomous aquatic surface vehicle for inspection and monitoring of wet nuclear storage facilities*, Robotics **8** (2019) 47.

[32] H.S. Kim, J.H. Ha, S.H. Park, S.Y. Cho and Y.K. Kim, *Fabrication and performance characteristics of a CsI(Tl)/PIN diode radiation sensor for industrial applications*, Appl. Radiat. Isot. **67** (2009) 1463.

[33] H.S. Kim, S.H. Park, J.H. Ha, D.-H. Lee and S.Y. Cho, *Characteristics of a fabricated PIN photodiode for a matching with a CsI(Tl) scintillator*, IEEE Trans. Nucl. Sci. **57** (2010) 1382.

[34] S. Jan et al., *GATE: A Simulation toolkit for PET and SPECT*, Phys. Med. Biol. **49** (2004) 4543 [physics/0408109].

[35] C. Bagatelas, C. Tsabaris, M. Kokkoris, C.T. Papadopoulos and R. Vlastou, *Determination of marine gamma activity and study of the minimum detectable activity (MDA) in* 4*pi geometry based on Monte Carlo simulation*, Environ. Monit. Assess. **165** (2010) 159.

[36] Y. Zhang, C. Li, D. Liu, Y. Zhang and Y. Liu, *Monte Carlo simulation of a NaI(Tl) detector for in situ radioactivity measurements in the marine environment*, Appl. Radiat. Isot. **98** (2015) 44.

[37] L.A. Currie, *Limits for qualitative detection and quantitative determination. Application to radiochemistry*, Anal. Chem. **40** (1968) 586.

[38] S. Koo, Y. Song, S.H. Lim, M.H. Oh, S.N. Seo and S. Baek, *Development of a remote supervisory control and data acquisition system for offshore waste final disposal facility*, J. Coastal Res. **90** (2019) 205.

[39] CHCNAV, *APACHE5 USV. Operation Manual*, CHCNAV, Shanghai China (2018).

[40] D. Tsumune, T. Tsubono, M. Aoyama and K. Hirose, *Distribution of oceanic* ^{137}*Cs from the Fukushima Dai-ichi Nuclear Power Plant simulated numerically by a regional ocean model*, J. Environ. Radioact. **111** (2012) 100.

[41] Korean Nuclear Safety and Security Commission, *2017 Annual report of oceanic environment radiation*, (2017) http://nsic.nssc.go.kr/nsic.do?nsicKey=20010503.

2020 JINST 15 P06027